Available online at www.sciencedirect.com
SCIENCE DIRECT®
Journal of the European Ceramic Society 24 (2004) 3559–3573
www.elsevier.com/locate/jeurceramsoc

Oxidation behaviour of a $MoSi_2$-based composite in different atmospheres in the low temperature range (400–550 °C)

K. Hansson [a,*], M. Halvarsson [b], J. E. Tang [b], R. Pompe [c], M. Sundberg [d], J.-E. Svensson [a]

[a] *Department of Environmental Inorganic Chemistry, Chalmers University of Technology, SE-412 96 Göteborg, Sweden*
[b] *Department of Experimental Physics, Chalmers University of Technology and Göteborg University, SE-412 96 Göteborg, Sweden*
[c] *Swedish Ceramic Institute, SE-412 96 Göteborg, Sweden*
[d] *Kanthal AB, Hallstahammar, Sweden*

Received 4 June 2003; received in revised form 20 November 2003; accepted 28 November 2003

Available online 15 April 2004

Abstract

The oxidation characteristics of a $MoSi_2$-based composite within the temperature range of 400–550 °C were investigated. The effects of temperature and water vapour on oxidation were examined. The oxidation kinetics were studied using a thermobalance, while the morphology and composition of the oxides were examined using XRD, ESEM/EDX, and SEM/EDX.

The peak oxidation rates in dry O_2 and $O_2 + 10\% H_2O$ were found to occur at temperatures of approximately 510 and 470 °C, respectively. Within the temperature range of accelerated oxidation (400–500 °C), the oxidation rate in $O_2 + 10\% H_2O$ was substantially higher than that in dry O_2. At higher temperatures, the oxidation rate decreased, and the magnitude of the decrease was steeper and occurred at a lower temperature for $O_2 + 10\% H_2O$ (510 °C) than for O_2 (550 °C). Furthermore, the rate of depletion of molybdenum (Mo) from the oxide scales during oxidation increased with increasing temperature and water vapour content. It appears that Mo loss is a key process influencing the protective properties of the oxide layer on the $MoSi_2$ composite. A potential mechanism for the different oxidation behaviours in O_2 and $O_2 + 10\% H_2O$ is proposed.

Keywords: $MoSi_2$; Corrosion; Silicides; SiO_2; Refractories

1. Introduction

The $MoSi_2$-based composite "Superkanthal 1800" is used as heating elements in industrial furnaces that are operated at temperatures up to 1800 °C. $MoSi_2$ is used in high-temperature applications because of its high melting point (2020 °C) and its excellent oxidation resistance at high temperatures (600–1800 °C), which is attributed to the formation of a protective self-healing silica scale. However, when $MoSi_2$ is oxidised at lower temperatures, i.e. between 400 and 600 °C, it undergoes severe corrosion and may disintegrate into powder.[1–3] This phenomenon was first described by Fitzer,[4] who termed it "$MoSi_2$ pest". At low temperature, $MoSi_2$ is oxidised as described by reaction (1)[5,6]

$$2MoSi_2(s) + 7O_2(g) \rightarrow 2MoO_3(s) + 4SiO_2(s), \quad \Delta G_{(500\,^\circ C)} = -4000\,kJ/mol \tag{1}$$

In the high-temperature range, reaction (1) occurs initially. However, the MoO_3 forms volatile species and evaporates, leaving behind an oxide layer of pure SiO_2. When the protective SiO_2 scale is established, the lowered partial pressure of oxygen at the bulk/oxide interface allows only Si to be oxidised, as described by reaction (2)[5,6]

$$5MoSi_2(s) + 7O_2(g) \rightarrow Mo_5Si_3(s) + 7SiO_2(s), \quad \Delta G_{(500\,^\circ C)} = -5200\,kJ/mol \tag{2}$$

It has been reported that the low temperature oxidation behaviour of $MoSi_2$ is a function of temperature, microstructure, composition, and atmosphere.[1,3,7–9] Accelerated oxidation and pesting is reported to be most severe around 500 °C in O_2 atmospheres.[1,7,8] In addition the cast material, which contains microcracks, undergoes accelerated oxidation and fragmentation. Hot, isostatically pressed, single-crystal material, which lacks microcracks, also undergoes accelerated oxidation but does not fragment.[3]

$MoSi_2$ is strictly stoichiometric according to the phase diagram, and thus the composite is liable to contain small

* Corresponding author.
E-mail address: krh@envic.chalmers.se (K. Hansson).

0955-2219/$ – see front matter © 2004 Elsevier Ltd. All rights reserved.
doi:10.1016/j.jeurceramsoc.2003.11.024

amounts of Mo_5Si_3 or Si. $MoSi_2$ that is manufactured with a slight excess of Mo yields a Mo_5Si_3 phase in the material, thereby preventing the presence of Si, which would reduce the mechanical properties of the material. On the other hand, it has been suggested that the existence of the Mo_5Si_3 phase promotes accelerated oxidation.[1,3]

It has been reported that the addition of 0.05 or 0.2 atm water vapor to the exposure air at 500 °C has no influence on the oxidation of fully dense $MoSi_2$.[9] On the other hand, when porous $MoSi_2$ is oxidised in the presence of water vapour, the oxidation rates increase with the partial pressure of H_2O, both during incubation and the accelerated oxidation periods. It has been speculated that the accelerated oxidation is due to the formation of the metastable hydrates $H_2Si_3O_7$ and $H_4Si_8O_{18}$ at the pores.[9]

In another investigation, the cyclic oxidation behaviour of a $MoSi_2$ composite was examined between 400 and 600 °C in dry air, wet air (0.028 atm water vapour), and oxygen.[1] In this case, the water vapour extended the incubation period, which was followed by linear oxidation at a rate that was roughly similar to that in dry air. These results suggest that the addition of water vapour retards the nucleation and growth of solid molybdenum oxides. The hydrated species $MoO_3{\cdot}H_2O(g)$ is formed, which has a higher vapour pressure than the $(MoO_3)_n$ species that form in dry O_2.[10]

Previously,[11,12] we examined the oxidation of $MoSi_2$ at 450 °C in O_2, O_2+2% H_2O, and O_2+10% H_2O, and showed that with increasing water vapour content the oxidation rate increased considerably, while the Mo content in the oxide scales decreased. The increased oxidation rate in the presence of water vapour was probably due to enhanced loss of Mo. As a result, an oxide scale with an open structure was formed, which facilitated the rapid inward diffusion of oxygen.

The aim of the present investigation was to further develop and examine our earlier proposed mechanism for the oxidation behaviour of a $MoSi_2$-based composite in the low temperature range, in both dry and wet O_2.[11] We examined how the Mo loss from the oxide scale varied according to changes in temperature and atmosphere. In addition, we studied the effects of Mo removal on the oxidation, microstructure, and morphology of the oxide scale.

2. Experimental

In this investigation a commercial clay-bonded $MoSi_2$-based composite (KS 1800) was examined. The composite is manufactured by mixing $MoSi_2$ powder, clay (bonding material), and water. The major components of the clay were SiO_2 and Al_2O_3. The mixture was extruded into 3 mm-diameter rods, dried, and then sintered at high temperatures. During the final step, a SiO_2 scale formed on the surface of the material. After sintering, the material was more than 99% dense, and consisted of a major $MoSi_2$ phase, approximately 3% Mo_5Si_3, and 10% bonding material (clay). The material was supplied in the form of 10 cm-long rods, which were sandblasted with 50 μm Al_2O_3 powder to remove the SiO_2 scale.

The rods were cut into 2.0–3.5 cm-long sections using a high-speed diamond saw. The cross-section surfaces were polished with 320-grit SiC paper. A 1.15-mm through-hole was drilled near one end of each specimen for thermogravimetric analysis (TGA). Before exposure, the specimens were cleaned ultrasonically, first with distilled water, followed by ethanol, and finally with acetone. The samples were then dried in flowing air and their weights were recorded before and after exposure.

The exposures were performed in a horizontal furnace that contained a 50-mm diameter SiO_2-glass tube or in a SETARAM TGA system. In the TGA system, the weight of the specimen was recorded as the specimen was exposed to the desired temperature and atmosphere. The exposures were carried out at 400–550 °C in a furnace system that was fitted with a humidifier, which produced a reaction gas consisting of O_2, O_2+10% H_2O (0.9 atm O_2+0.1 atm H_2O), Ar, Ar + 10% H_2O, and Ar + 40% H_2O flowing gases.

Before investigating the cross-section of the oxide scale, the samples were polished using increasingly finer grades of diamond suspension, finishing at 1 μm. The samples were then carbon-coated.

The microstructures of the cross-sections of the oxide scales were examined with a Camscan S4-80DV scanning electron microscope (SEM), using the back-scattered electron imaging mode. The SEM was equipped with the Link eXL energy dispersive X-ray (EDX) spectroscopy system. Accelerating voltages of 8 and 20 kV were used for the SEM imaging and SEM/EDX analyses, respectively. The morphologies of the scales were examined with the ElectroScan 2020 environmental scanning electron microscope (ESEM) in the secondary electron mode. The ESEM was equipped with a Link Isis EDX system. An accelerating voltage of 20 kV was used. Analyses of the crystalline phases in the oxide scales were performed using the Siemens D5000 X-ray diffractometer (XRD) with the grazing-incidence set-up. Incidence angles of 1–10° were used, depending on the oxide scale thickness.

3. Results and discussion

3.1. Kinetics

The oxidation kinetics of the $MoSi_2$ composite in O_2 and O_2 + 10% H_2O were examined by thermogravimetric exposures, as shown in Figs. 1 and 2.

The mass gain due to oxidation of the $MoSi_2$ composite in dry O_2 increased as the temperature rose from 400 up to 510 °C, and then decreased rapidly (Fig. 1). In some cases, signs of spallation were noted around the edges of the drilled hole, where the sample may have suffered mechanical damage. The increase in mass up to 510 °C is consistent with

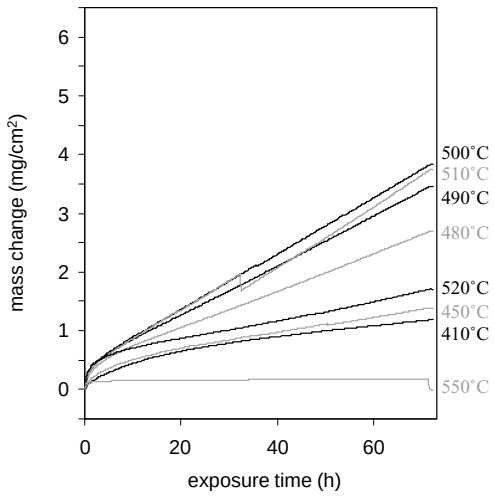

Fig. 1. The mass changes of the $MoSi_2$-based composite that was oxidised in a thermobalance in an atmosphere of dry oxygen at different temperatures.

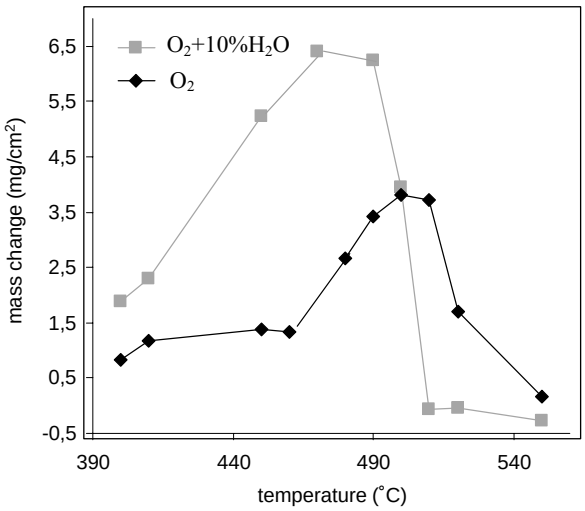

Fig. 3. The mass changes of a $MoSi_2$-based composite that was exposed for 72 h in O_2 and $O_2 + 10\% H_2O$ at different temperatures, revealing the peak oxidation temperatures.

the fact that the rate of reaction increases with temperature. However, in order to interpret the decrease in mass above 510 °C, it was necessary to investigate the microstructures of the oxide scales (see Section 3.2).

The observation of the above-mentioned peak oxidation temperature is in agreement with previous reports.[1,7,8] However, in these previous studies, only a rough estimation of the peak oxidation temperature was given, and the link between peak oxidation temperature and exposure atmospheres was not considered.

The mass gain due to the oxidation of the $MoSi_2$ composite in $O_2 + 10\% H_2O$ increased at temperatures from 400 up to 470–490 °C (Fig. 2). The mass gain then dropped off rapidly at temperatures above 500 °C, at which temperature completely different oxidation kinetics were observed. The samples that were oxidised at or above 510 °C initially gained mass, then decreased in mass, and eventually showed

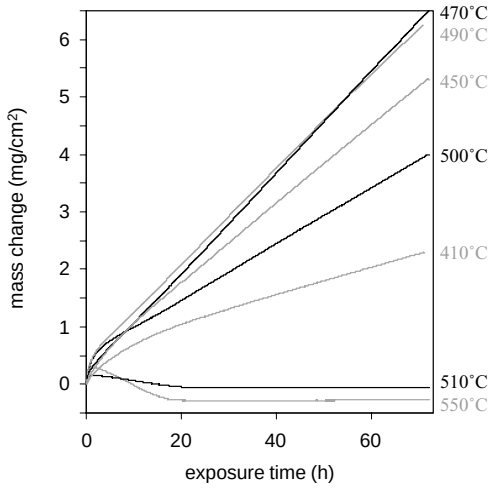

Fig. 2. The mass changes of the $MoSi_2$-based composite that was oxidised in a thermobalance in $O_2 + 10\% H_2O$ at different temperatures.

an increase in mass, although at a substantially lower rate. The observed decrease in mass represents evaporation from the sample.

In Fig. 3, the mass gain of samples that were oxidised in the thermobalance for 72 h at different temperatures is summarised. It is evident that the temperature region in which accelerated oxidation took place was shifted towards lower temperatures in $O_2 + 10\% H_2O$ (400–510 °C) compared with oxidation in O_2 (400–550 °C). Furthermore, the oxidation rate in this "accelerated oxidation rate region" was higher in $O_2 + 10\% H_2O$ than in O_2.

Since the oxidation rate was higher in O_2 when water vapour was present than in dry O_2, we investigated whether the water itself oxidised the material. Calculation of the free energy of formation shows that reaction (3) is possible:

$$MoSi_2 + 7H_2O \rightarrow MoO_3 + 2SiO_2 + 7H_2, \quad \Delta G_{(450\,^\circ C)} = -550\,\text{kJ/mol} \tag{3}$$

Exposures were performed at 450 °C in dry argon as well as in argon with different amounts of water vapour (Fig. 4). The rates of oxidation in O_2 and $O_2 + 10\% H_2O$ at identical temperatures are also shown for comparison. Negligible mass gains were recorded for exposures in argon and argon/H_2O mixtures. The small mass gains observed were probably due to oxygen leakage into the system when the samples were placed in the furnace. Thus, it seems likely that water does not oxidise $MoSi_2$, at least not to any significant extent. Therefore, an alternative mechanism is needed to explain the increased oxidation rate of the $MoSi_2$ composite in O_2 when water vapour is present.

3.2. Oxide scale morphology and composition

Samples that were oxidised in dry O_2 or $O_2 + 10\% H_2O$ for 72 h at (a) 410 °C, (b) 450 °C, (c) 490 °C, (d) 520 °C,

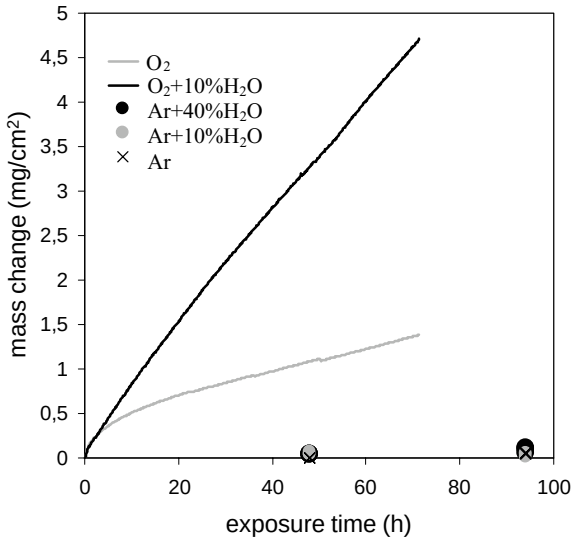

Fig. 4. The mass changes of a $MoSi_2$-based composite that was exposed at 450 °C in Ar, Ar + 10% H_2O, Ar + 40% H_2O, O_2, and O_2 + 10% H_2O. The small mass gains following exposure in the Ar/H_2O mixtures shows that the increased oxidation rate in O_2 + 10% H_2O compared to O_2 is not due to water oxidation.

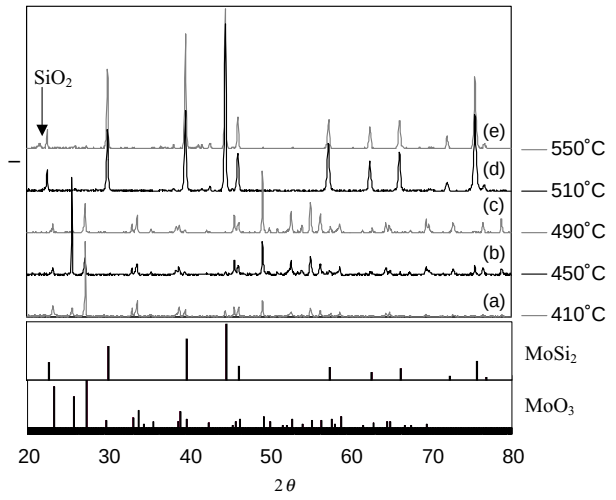

Fig. 6. XRD diffractograms for samples that were exposed for 72 h in O_2 + 10% H_2O at 410–550 °C. Samples that were oxidised at 410–500 °C contain crystalline MoO_3. The samples that were oxidised at higher temperatures yield XRD diffractograms that are similar to those of the unexposed materials ($MoSi_2$ and Mo_5Si_3). The oxide scale probably consists of amorphous SiO_2. At 550 °C, the peak at $2\theta = 22.6°$ indicates the formation of crystalline SiO_2.

and (e) 550 °C were analysed using XRD and ESEM/EDX. The XRD diffractograms, together with the peak positions and intensities for $MoSi_2$ and MoO_3 are shown in Figs. 5 and 6. The additional peaks, which are not attributable to either $MoSi_2$ or MoO_3, are due to the Mo_5Si_3 phase in the bulk material.

The oxide scales of the samples that were oxidised in dry O_2 contained crystalline MoO_3 at all temperatures studied. Previously, it was shown using TEM that the oxide consisted

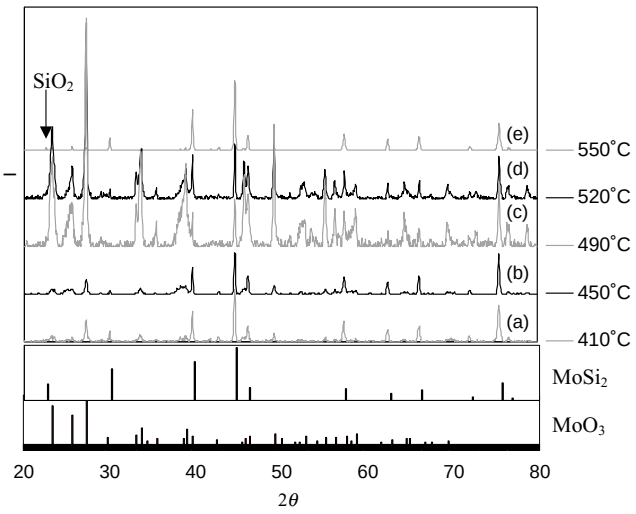

Fig. 5. XRD diffractograms of samples that were exposed for 72 h in O_2 at 410–550 °C. The XRD peaks for $MoSi_2$ and MoO_3 are shown. However, there are some additional peaks in the diffractograms. These peaks are due to the Mo_5Si_3 phase in the bulk material. The XRD diffractograms show that the samples contain crystalline MoO_3 at all temperatures. At 550 °C, the peak at $2\theta = 22.6°$ indicates that crystalline SiO_2 has formed.

of nanometer-sized MoO_3 particles that were embedded in an amorphous SiO_2.[13] The mass change measurements indicated that the oxide scale thickness increased from 400 up to 500 °C in dry O_2, and then decreased at higher temperatures. The XRD diffractogram gave similar results. The MoO_3 peaks grew relative to the substrate peaks from 400 to 490 °C, and then decreased at higher temperatures (Fig. 5).

The samples that were oxidised in O_2 + 10% H_2O at 400–500 °C contained crystalline MoO_3 (Fig. 6). The samples that were oxidised at higher temperatures yielded a similar XRD diffractogram as the unexposed material ($MoSi_2$ and Mo_5Si_3). Thus, the oxide scale probably consisted of amorphous SiO_2. At 550 °C, a peak at $2\theta = 22.6°$ indicated the formation of crystalline SiO_2. This peak was also found after exposures in O_2 at the same temperature. Therefore, it appears that this higher temperature allows some of the SiO_2 to restructure into the crystalline phase. These results show there are two different oxidation regimes in O_2 + 10% H_2O: one at temperatures up to around 500 °C, in which MoO_3 is found in the oxide scale; and another at higher temperatures, in which no MoO_3 is found in the scale. This is consistent with the reaction kinetics shown in Fig. 2.

The XRD results are consistent with the ESEM images of the surfaces of the oxide scales that were formed in O_2 and O_2 + 10% H_2O (Figs. 7 and 8). Needle-shaped MoO_3 crystals (arrows) are visible on all the surfaces of the MoO_3-containing samples. Amorphous-like lumps (marked with circles) are visible on all the samples. However, these lumps are smaller on the sample that was oxidised at 550 °C in dry O_2, and the silica scale appears denser. This probably enhances the protective properties of the oxide scale, which is consistent with the kinetics shown in Fig. 2.

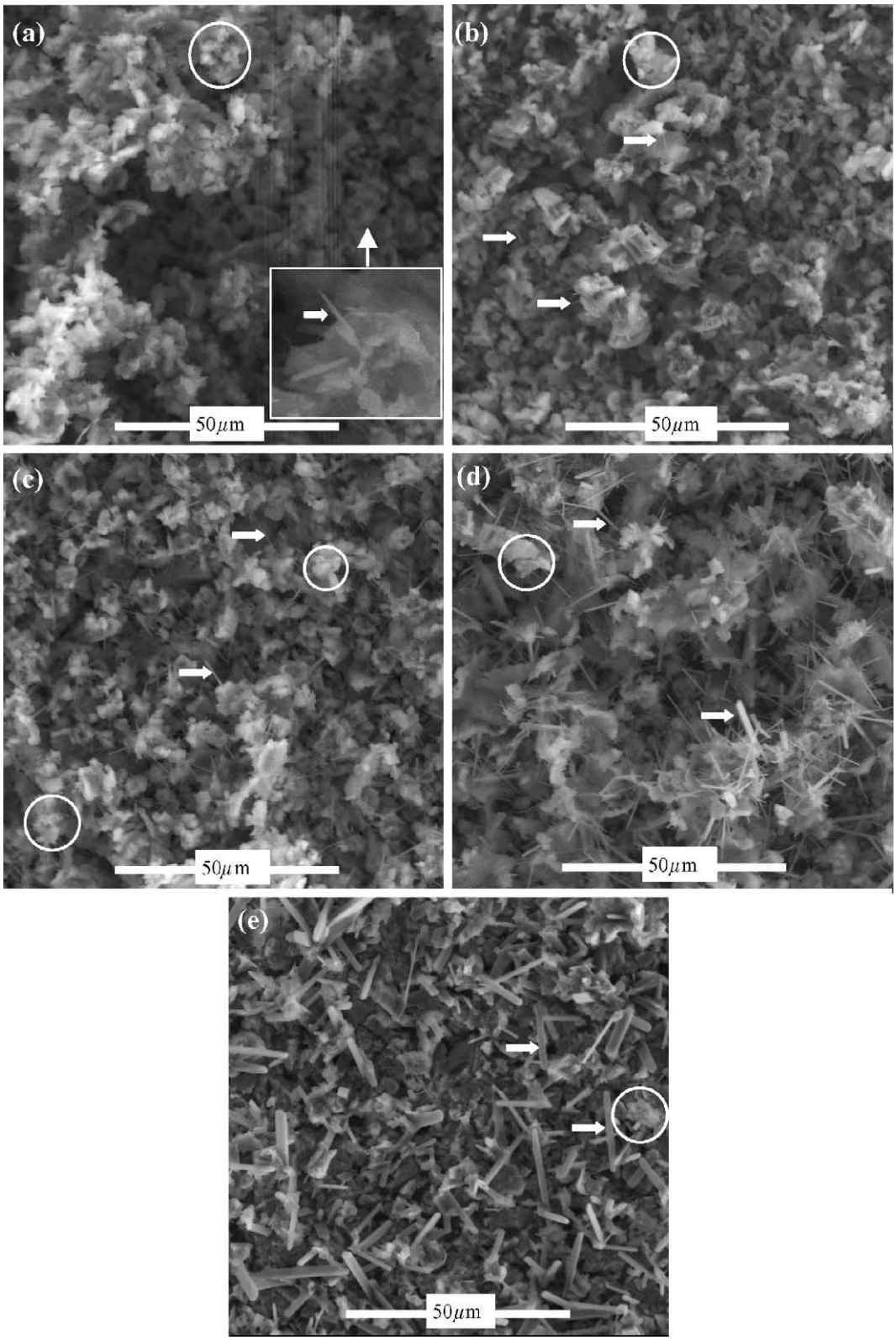

Fig. 7. ESEM images of the surface oxides of samples that were oxidised in dry oxygen for 72 h at (a) 410 °C, (b) 450 °C, (c) 490 °C, (d) 520 °C, and (e) 550 °C. MoO_3 crystals (arrowed) are visible on all the surfaces. In addition, amorphous-like lumps (marked with circles) are visible on all the samples. The silica scale no longer has a diffuse amorphous shape and appears denser at 550 °C.

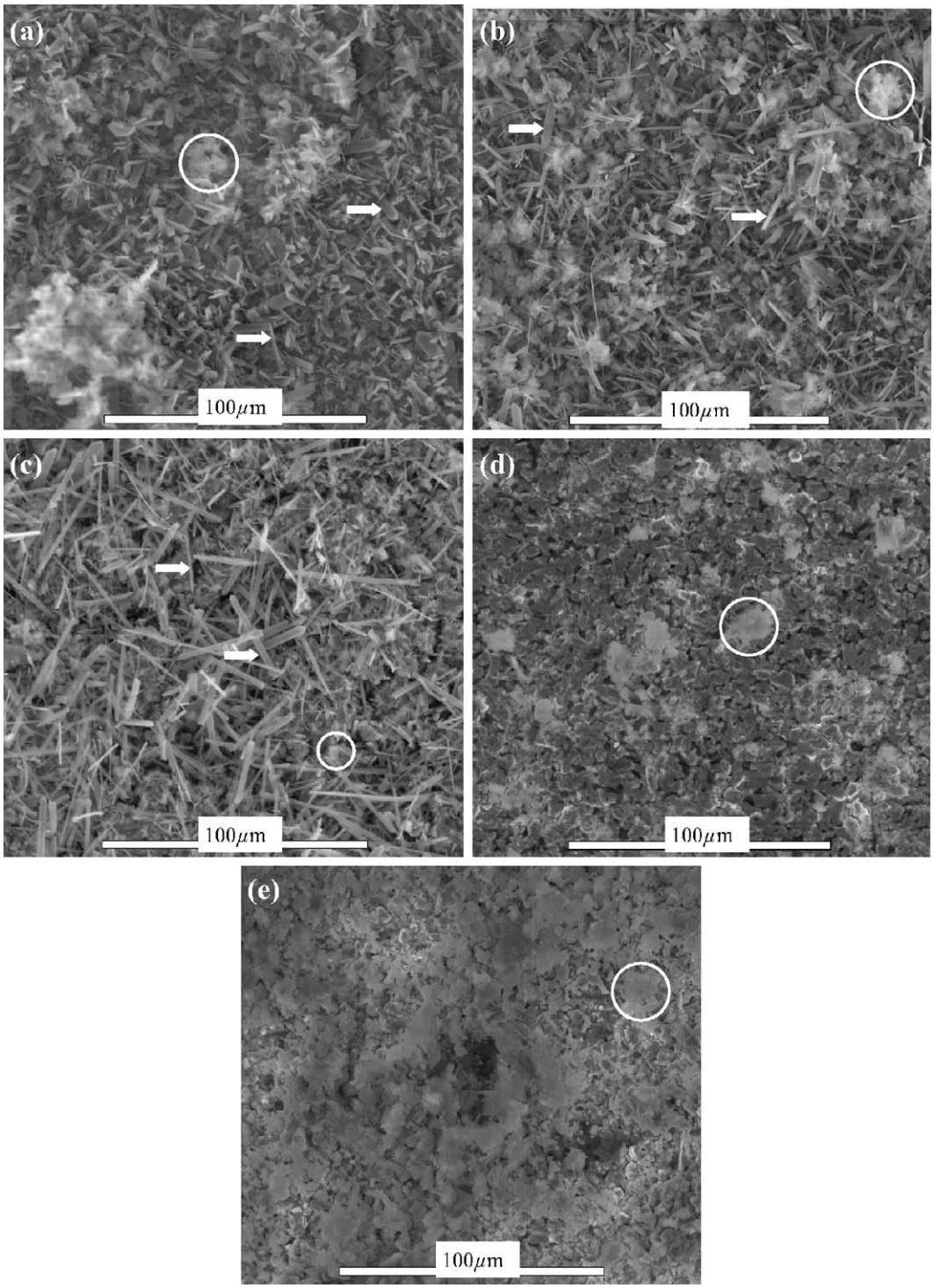

Fig. 8. ESEM images of the surfaces of the oxide scales of samples that were oxidised in $O_2 + 10\% H_2O$ for 72 h at (a) 410 °C, (b) 450 °C, (c) 490 °C, (d) 520 °C, and (e) 550 °C. Needle-shaped MoO_3 crystals (arrows) are visible on the samples that were oxidised at temperatures between 410 and 500 °C. Amorphous-like lumps (marked with circles) are visible on all the sample surfaces. The surfaces of the samples that were oxidised above 510 °C appear to be covered with dense oxide scales, with only a few amorphous SiO_2 lumps and no MoO_3 crystals.

The samples that were oxidised in $O_2 + 10\% H_2O$ at temperatures above 500 °C initially gained mass, then decreased in mass, and finally, tended to increase in mass again, although at a substantially lower rate. In order to better understand this initial oxidation mechanism, three samples were exposed at 520 °C in the thermobalance. One sample was exposed for 1 h, at which time the initial mass gain had stopped. Another sample was oxidised for 18 h, at which time the loss of mass ceased, and a third sample was oxidised for 72 h. The mass–change curve, together with ESEM

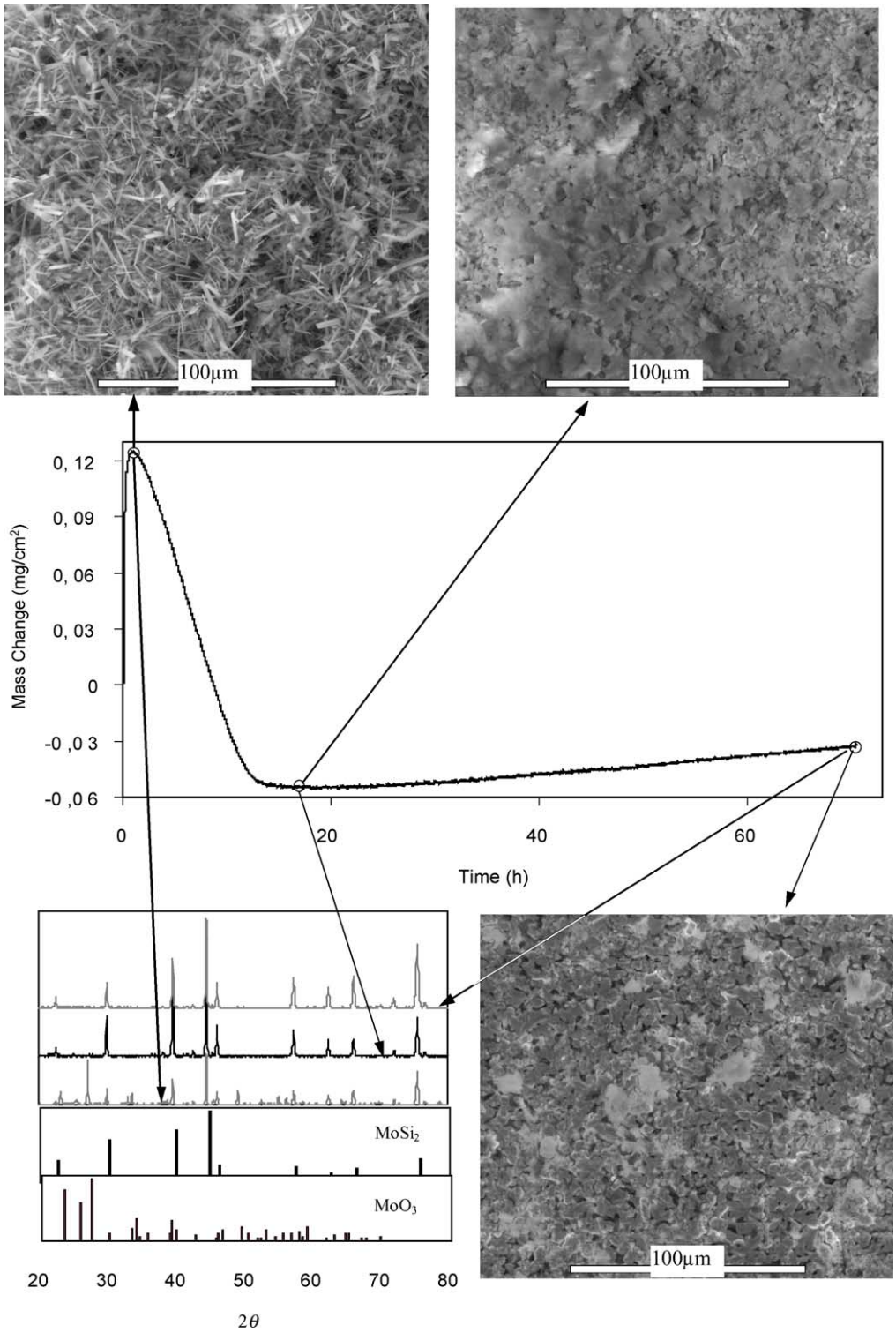

Fig. 9. The oxidation process for up to 72 h of exposure at 520 °C in $O_2 + 10\% H_2O$ is shown. Three samples were exposed. One sample was exposed for 1 h, at which time the initial mass gain had stopped. Another sample was oxidised for 18 h, at which time the loss of mass ceased, and a third sample was oxidised for 72 h. The XRD diffractogram shows MoO_3 on the sample that was oxidised for 1 h. This is confirmed by the ESEM image, in which MoO_3 crystals and amorphous SiO_2 clusters clearly cover the surface. In the sample that was oxidised for 18 h, MoO_3 was not detected by XRD, and no crystals are observed on the surface by ESEM. This indicates that the initial mass gain is due to the formation of MoO_3, and that the subsequent mass loss is due to the loss of MoO_3.

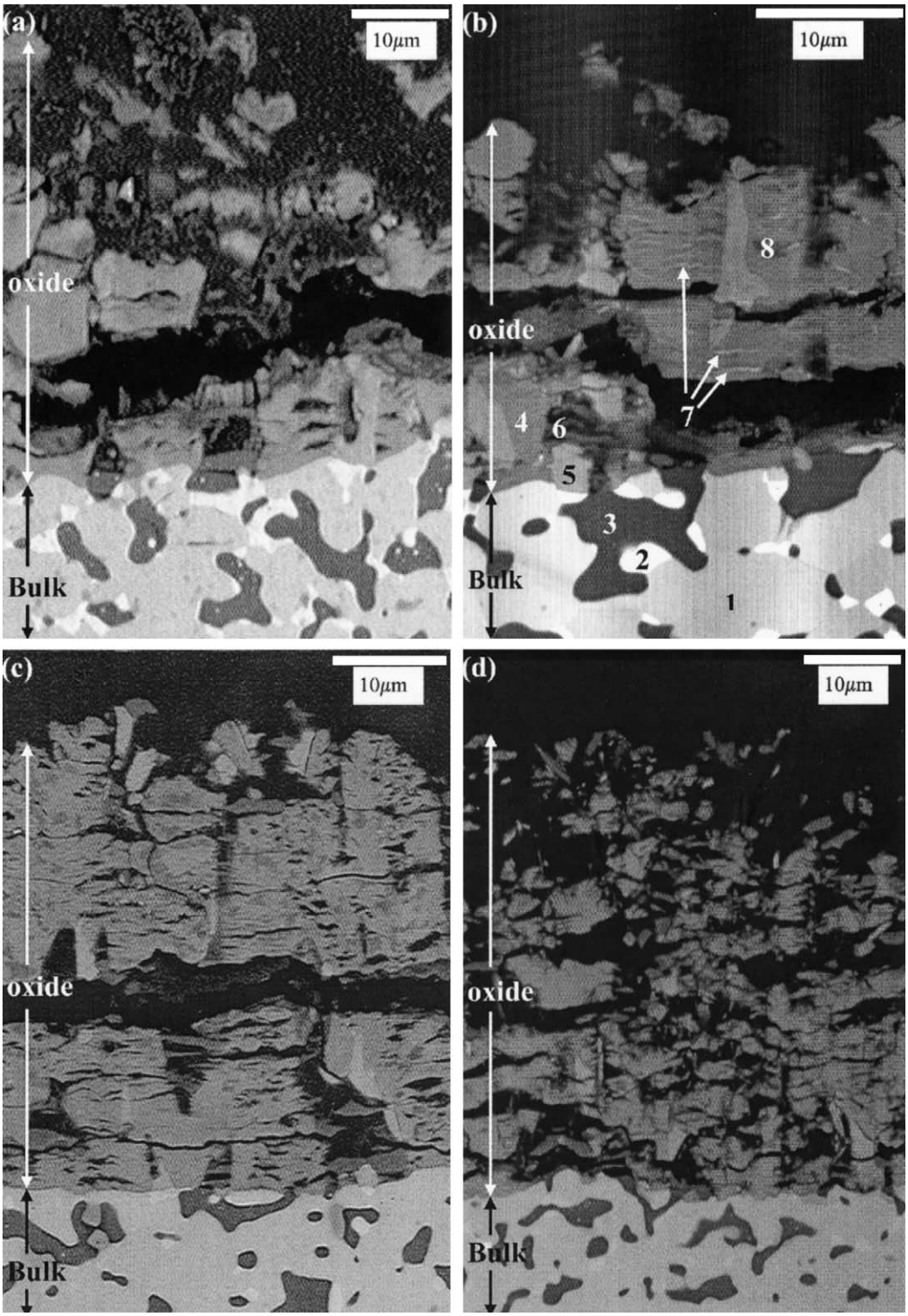

Fig. 10. SEM images of the cross-sections of samples that were exposed in dry O_2 for 72 h at (a) 410 °C, (b) 450 °C, (c) 490 °C, (d) 520 °C, and (e) 550 °C. The major grey region (1) is the $MoSi_2$, the white islands (2) are Mo_5Si_3, and the black islands (3) are clay. The major medium-grey regions (4) are toxidised $MoSi_2$ (nanometer-sized MoO_3 particles in amorphous SiO_2), and the light-grey regions (5) are oxidised Mo_5Si_3 (nanometer-sized MoO_3 particles in amorphous SiO_2). The black regions (6) are the clay. The white strips (7) represent agglomerated MoO_3 crystals. The dark-grey regions (8) consist of Mo-depleted oxidised $MoSi_2$ or Mo_5Si_3.

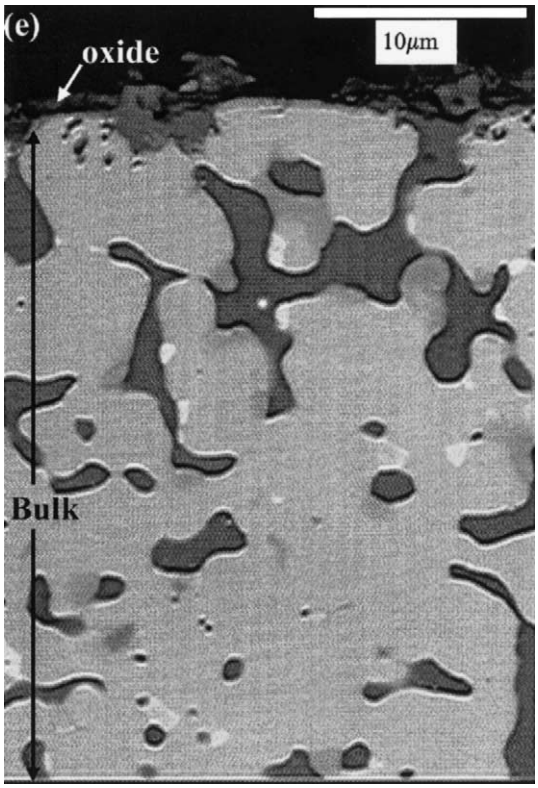

Fig. 10. (*Continued*).

images of the surface oxide scales and XRD diffractograms, is shown in Fig. 9. The XRD diffractogram shows the presence of MoO_3 on the sample that was oxidised for 1 h. This finding was confirmed by the ESEM image, in which MoO_3 crystals and amorphous SiO_2 lumps covered the surface. However, MoO_3 was not detected on the samples that were oxidised for 18 or 72 h, and no crystals were observed on the surface. This indicates that the initial mass gain is due to the formation of MoO_3 and SiO_2, and that the subsequent mass loss is due to the loss of MoO_3.

3.3. Microstructure of cross-sections

The general trend towards the appearance of oxide scales of $MoSi_2$ composite in O_2 was also noted in $O_2 + 10\% H_2O$ (Figs. 10 and 11). The oxide scales increased in thickness up to the temperature of the peak oxidation rate (470 °C in $O_2 + 10\% H_2O$; 500 °C in O_2). At higher temperatures, the oxidation rates slowed and the oxide scales became thinner.

The cross-sectional microstructures of the oxides of the $MoSi_2$ composite samples that were oxidised for 72 h at different temperatures in O_2 and $O_2 + 10\% H_2O$ were examined using SEM/EDX (Figs. 10 and 11).

The different regions in the bulk are indicated in Fig. 10b. The major grey region (1) is $MoSi_2$, the white islands (2) are Mo_5Si_3, and the black islands (3) are clay. Three of the regions in the oxide scale can be related directly to regions in the bulk. In Fig. 10, the major medium-grey regions (4) are oxidised $MoSi_2$, which have been shown previously to contain nanometer-sized MoO_3 particles in amorphous SiO_2.[13] The light-grey regions (5) represent oxidised Mo_5Si_3, which also consists of nanometer-sized MoO_3 particles in amorphous SiO_2. The black regions (6) represent clay that is trapped in the oxide scale. Two other regions are found in the oxide scale: white strips (7) of agglomerated MoO_3 crystals in the oxidised $MoSi_2$; and dark-grey regions (8) that consist of Mo-depleted oxidised $MoSi_2$ or Mo_5Si_3. These regions are composed primarily of SiO_2. A clearly visible dark-grey region (8) is also evident in Fig. 11a. Many large and small lateral cracks are visible in the oxides. This may be an effect of the oxidation and/or cooling. The volume increased about four times, during conversion from $MoSi_2$ to MoO_3 and SiO_2, thereby creating stresses in the oxide scale. The clay, which had about the same volume in the oxide as in the bulk, cracked due to this stress. The oxide scale may also have been subjected to stresses upon cooling, due to the different coefficients of thermal expansion between the bulk and the scale.

Upon initial oxidation of the $MoSi_2$-composite, some of the Mo was lost (medium-grey region). The loss of Mo in these regions depends on the oxidation atmosphere and temperature. During the continuous oxidation process, some of these regions lose almost all of their Mo content (dark-grey region), in what appears to be an inward-moving front as illustrated in Fig. 12. The size and number of these regions depend on the oxidation time, temperature, and atmosphere.

In the comparisons of the oxide scales that were formed in O_2 and $O_2 + 10\% H_2O$ at temperatures up to 520 and 500 °C, respectively, EDX shows that the oxidised $MoSi_2$ (medium-grey region) tends to be somewhat depleted of Mo. In the oxide scales that were formed in O_2, less than 10% of the total Mo was lost compared to about 20% loss in $O_2 + 10\% H_2O$. Mo depletion tended to increase with increasing temperature in $O_2 + 10\% H_2O$. This tendency was not as pronounced in O_2. The oxidised Mo_5Si_3 regions also showed the same tendency towards Mo loss. The dark-grey regions appear mostly in the outer part of the oxide scales and around cracks, where it is presumably easier for the Mo to escape. These regions are larger and more numerous in the oxide scales that were formed in $O_2 + 10\% H_2O$ (Fig. 11) than those that were formed in O_2 (Fig. 10). At temperatures above 520 °C in O_2 and 500 °C in $O_2 + 10\% H_2O$, the oxide scales were very thin. Thus, although EDX measurements became difficult, the scale was found to consist of almost pure SiO_2.

The above-mentioned results show that the Mo depletion is greater in the scales that are formed in $O_2 + 10\% H_2O$. Thus, it appears that the differences between the "accelerated oxidation rate regions" in O_2 and $O_2 + 10\% H_2O$ are linked to the rate of Mo removal. Whether or not Mo removal results in the oxide becoming more or less protective depends on the oxidation temperature, as illustrated in Fig. 13.

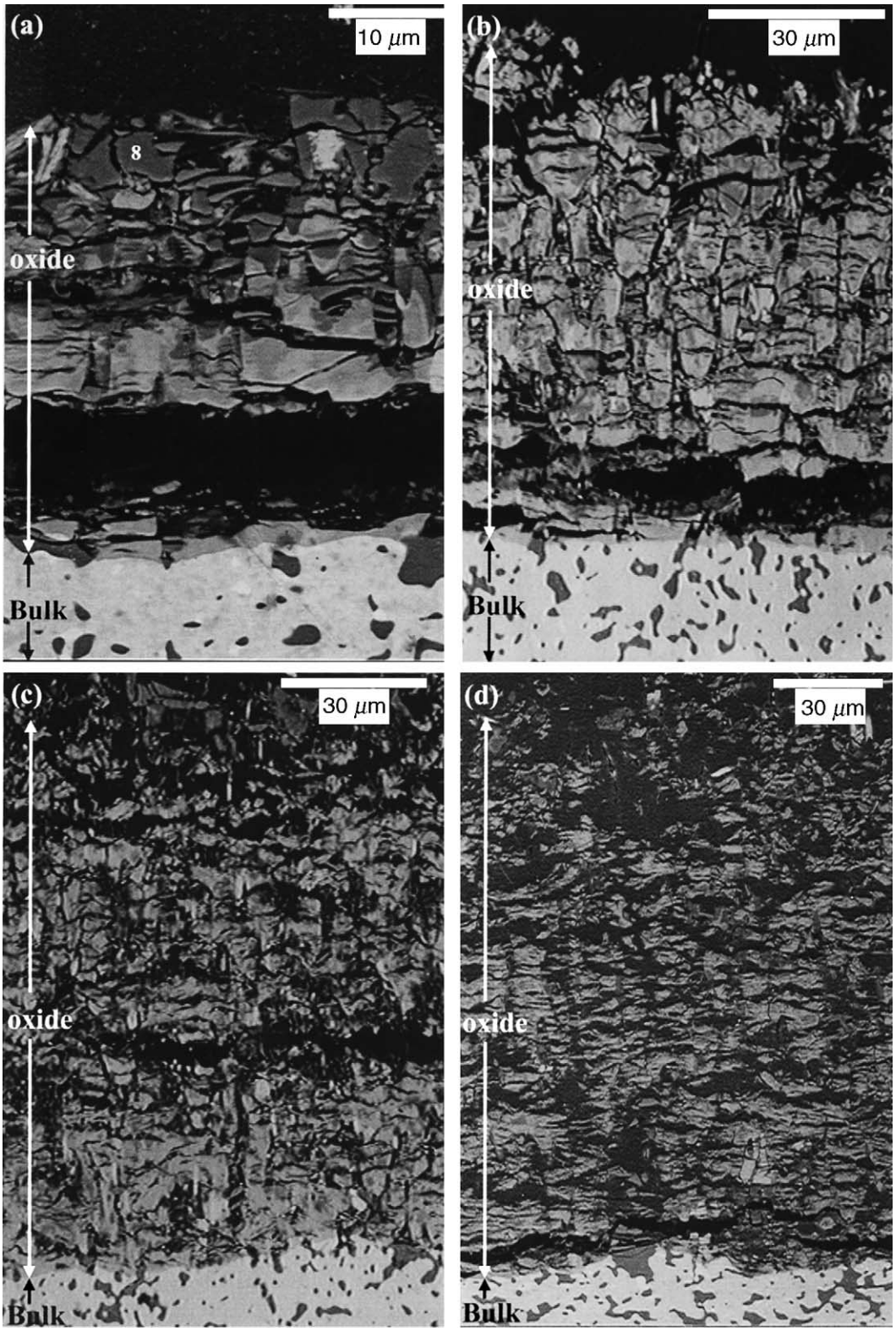

Fig. 11. SEM images of the cross-sections of the oxides of samples that were exposed in $O_2 + 10\% H_2O$ for 72 h at (a) 410 °C, (b) 450 °C, (c) 470 °C, (d) 490 °C, and (e) 520 °C. The dark-grey regions (8) consist of Mo-depleted oxidised $MoSi_2$ or Mo_5Si_3 (nanometer-sized MoO_3 particles in amorphous SiO_2).

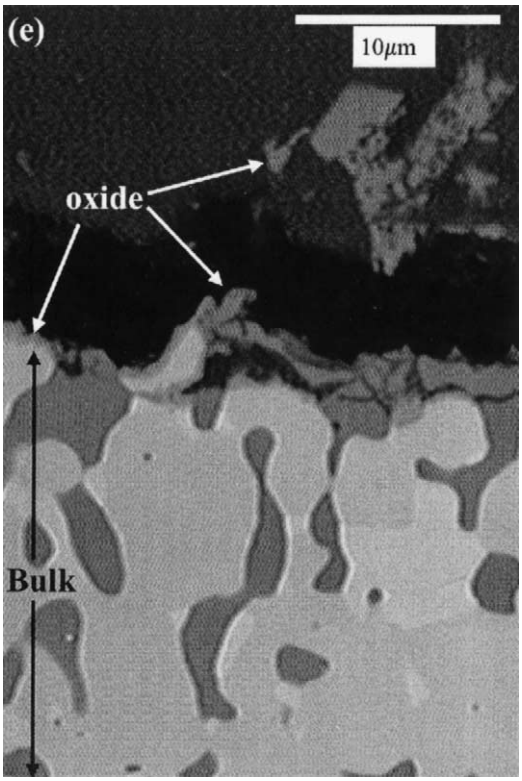

Fig. 11. (*Continued*).

At low temperatures (below ~510 °C in $O_2 + 10\% H_2O$ and 550 °C in O_2), Mo removal results in an oxide scale with an open structure. This facilitates the rapid diffusion of oxygen through the oxide scale, and the oxidation rate increases. At high temperatures (above ~510 °C in $O_2 + 10\% H_2O$ and 550 °C in O_2), diffusion within the SiO_2 scale appears to be sufficiently high to heal the voids left behind after the removal of Mo. This results in a dense protective scale that decreases the oxidation rate.

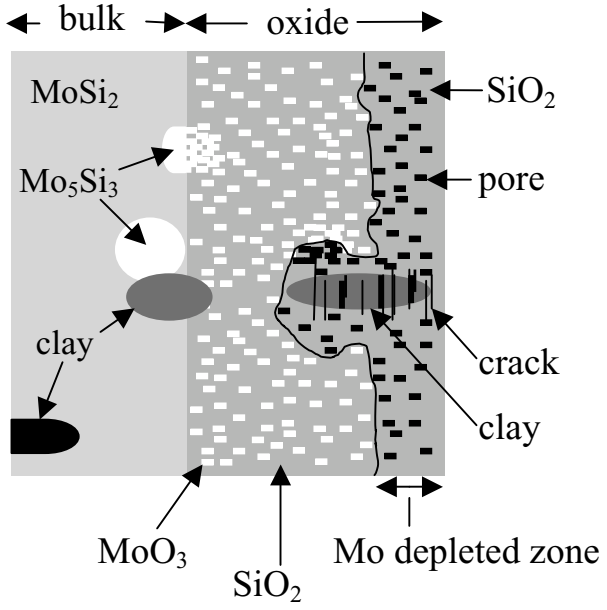

Fig. 12. Illustration of an inward-moving front of MoO_3 depletion in oxidised $MoSi_2$.

3.4. Evidence of Mo evaporation

During the $MoSi_2$ composite oxidation tests, particles were deposited downstream, in the cooler parts of the exposure tube. The extent of deposition was larger during oxidation in $O_2 + 10\% H_2O$ than in O_2. XRD analysis of particles that were collected after oxidation in $O_2 + 10\% H_2O$ at 450 °C showed the presence of MoO_3. The presence of amorphous SiO_2 was ruled out by EDX analysis. This shows that Mo-containing species evaporate when $MoSi_2$ is oxidised.

We have shown that Mo leaves the oxide in both O_2 and $O_2 + 10\% H_2O$ atmospheres, although to different extents. The oxides that are formed in $O_2 + 10\% H_2O$ are more highly Mo-depleted and a higher level of deposit are found downstream the samples after these exposures than the exposures in O_2. In the literature, it has been reported that the most abundant vapour species over MoO_3 powder at 850 °C are $(MoO_3)_3$, $(MoO_3)_4$, and $(MoO_3)_5$ at a ratio of about 20:7:1.[14] However, the atmosphere was not specified in that study. Another study showed that water vapour enhanced the volatility of MoO_3,[10] presumably due to the formation of $MoO_2(OH)_2$.[15]

In order to determine how Mo is volatilised from the oxide scale, we determined the amount of Mo that was deposited downstream and made thermodynamic calculations. The amount of evaporated Mo was determined using AAS to be approximately 1.4 mg after 94 h of exposure in $O_2 + 10\% H_2O$ at 450 °C with a gas flow of 150 ml/min. The equilibrium partial pressures were calculated at different temperatures for $(MoO_3)_3$ in dry O_2 and for $MoO_2(OH)_2$ in $O_2 + 10\% H_2O$. Tabulated Gibbs energies of formation were used in the calculations,[16,17] and the results are shown in Fig. 14. The total vapour pressure of the $(MoO_3)_3$ species at 450 °C was 3.1×10^{-11} atm, which gives a maximum deposition of 0.16 μg MoO_3 (gas flow = 150 ml/min; time = 94 h; pO_2 = 1 atm). The actual deposition is 4 orders of magnitude greater. This indicates that another species, which is more volatile than $(MoO_3)_3$, accounts for most of the Mo transport. Quantum chemical calculations show that $MoO_2(OH)_2$ is more stable than $(MoO_3)_3$ in the presence of water vapour,[18] that only a small activation energy is needed to form $MoO_2(OH)_2$.[18] In Fig. 14, the vapour pressure of $MoO_2(OH)_2$ species at 450 °C and 0.1 atm H_2O is shown as 6.3×10^{-7} atm, which gives a maximum deposition of 3.1 mg MoO_3 under the same experimental conditions as above (gas flow = 150 ml/min; time = 94 h; pH_2O = 0.1 atm). This is of the same order of magnitude as the amount of deposit found in reality, which indicates that $MoO_2(OH)_2$ is the volatile species. Therefore, we propose that Mo transport in the presence of

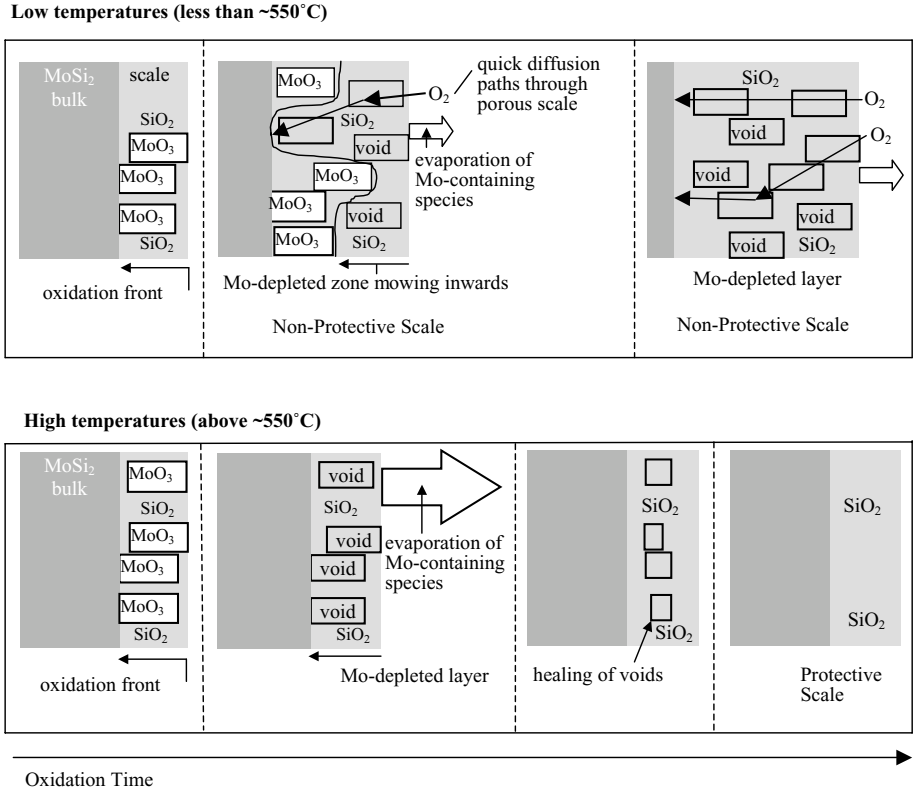

Fig. 13. Schematic illustration of the mechanism of high- and low-temperature oxidation of the $MoSi_2$ composite. At low temperatures (below ~550 °C), the removal of Mo results in an oxide scale with an open structure. This facilitates the rapid diffusion of oxygen through the oxide, and increases the oxidation rate. At high temperatures (above ~550 °C), the diffusion within the SiO_2 scale appears to be sufficiently rapid to heal the voids left behind after the removal of Mo. This results in a dense protective scale that decreases the oxidation rate.

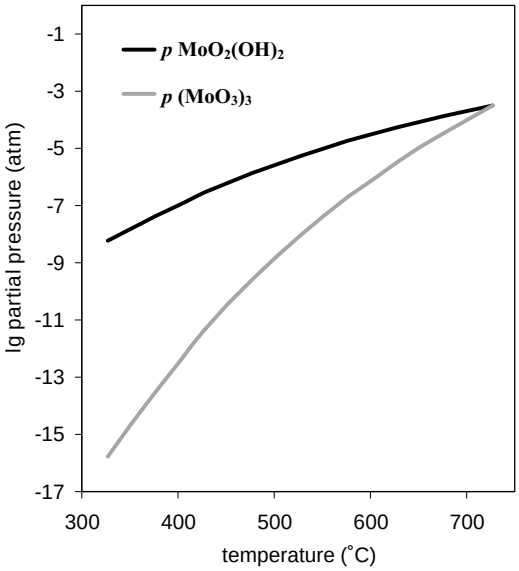

Fig. 14. The equilibrium partial pressures of $MoO_2(OH)_2$ in O_2+10% H_2O and $(MoO_3)_3$ in O_2 at different temperatures.

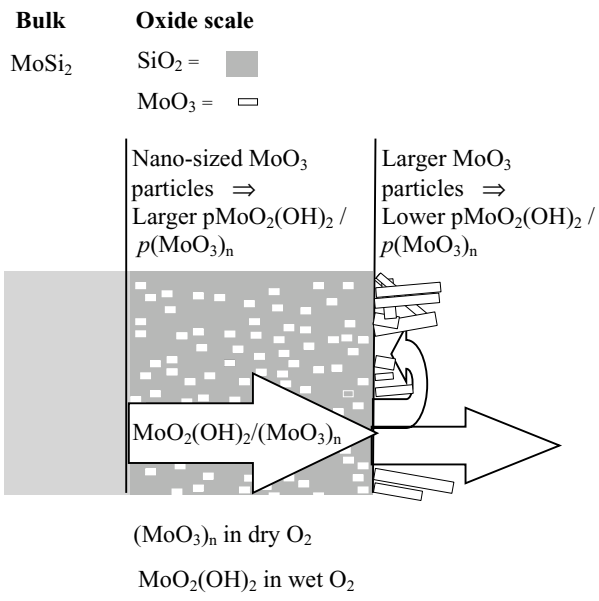

Fig. 15. Schematic picture of the equilibrium partial pressure of $MoO_2(OH)_2$ inside and outside the oxide of $MoSi_2$. The $pMoO_2(OH)_2$ within the oxide structure is higher due to the presence of nanometer-sized MoO_3 particles. When this vapour with its high $pMoO_2(OH)_2$ reaches the oxide surface, where a lower $pMoO_2(OH)_2$ prevails, some of the MoO_3 is re-deposited on the oxide surface.

water vapour can be explained by the following reaction (4):

$$MoO_3(s) + H_2O(g) \leftrightarrow MoO_2(OH)_2(g) \quad (4)$$

3.5. MoO_3 deposition on the oxide scale and exposure tube

MoO_3 crystals appeared on the surfaces of samples that were oxidised in $O_2 + 10\% H_2O$ between 400 and 510 °C

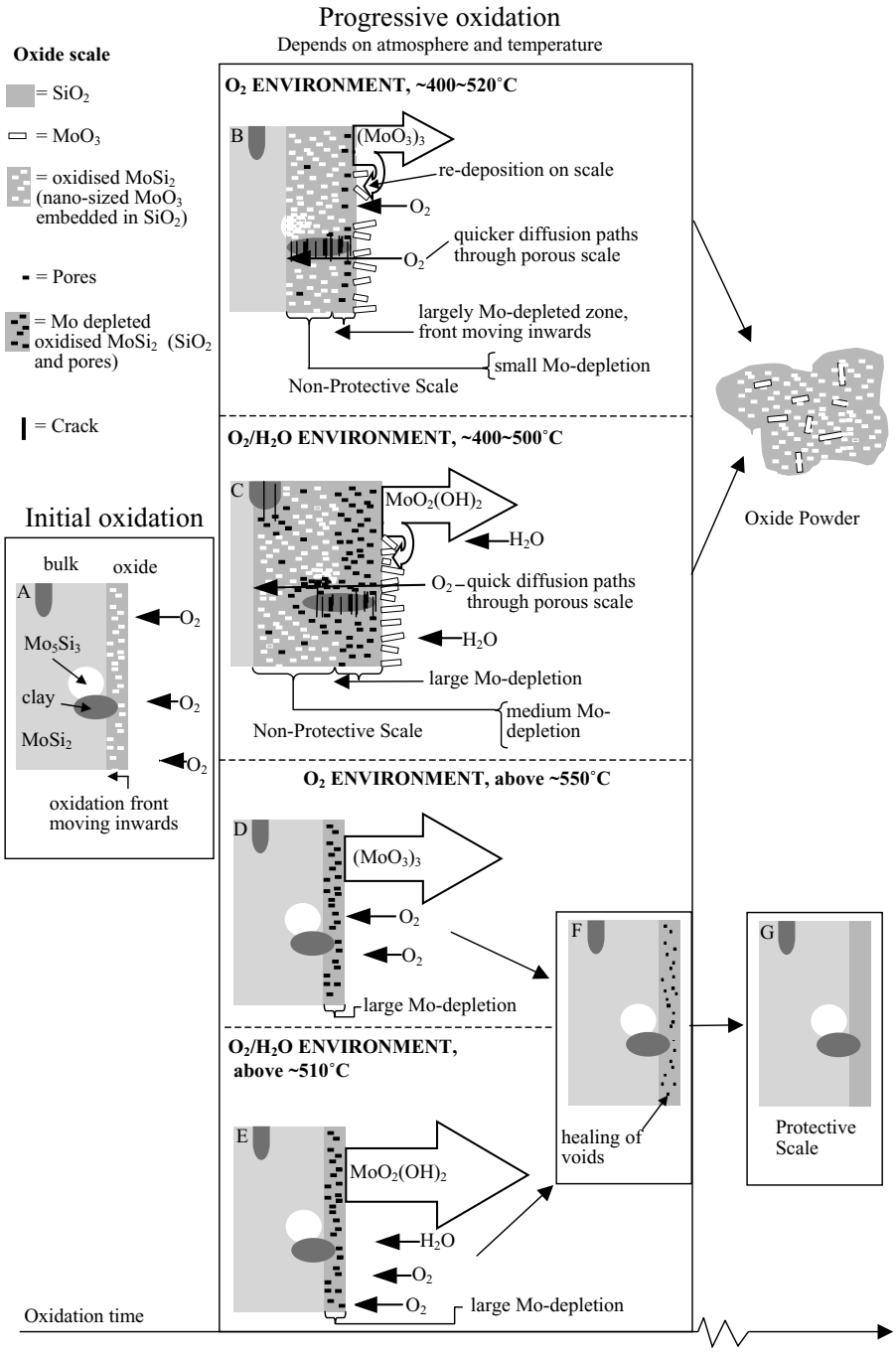

Fig. 16. Schematic picture of the hypothesis regarding the oxidation of $MoSi_2$ in dry O_2 and $O_2 + 10\% H_2O$ at temperatures between 410 and 550 °C. (A) $MoSi_2$ is oxidised to MoO_3 and SiO_2. (B, D) In dry oxygen, some of the MoO_3 agglomerates to the volatile $(MoO_3)_3$-species. (C, E) In O_2/H_2O mixtures, some of the solid MoO_3 reacts with water to form the volatile $MoO_2(OH)_2$-species. This results in the loss of Mo from the oxide. (B, C) At "low" temperatures (in O_2 up to ~520 °C; in $O_2 + 10\% H_2O$ up to ~500 °C), the loss of Mo leaves the oxide with an open structure, which facilitates the rapid diffusion of oxygen through the oxide. As a result, the oxidation rate increases. (D, E) At higher temperatures (in O_2 above ~550 °C; in $O_2 + 10\% H_2O$ above ~510 °C), more Mo is removed from the oxide, and the diffusion of the almost pure SiO_2 is sufficiently high to restructure and heal the pores (F). (G) As a result, a protective SiO_2 scale forms and the oxidation rate of $MoSi_2$ decreases.

and in O_2 between 400 and 550 °C. This behaviour can be explained by the thermodynamics of the surface energies. The equilibrium vapour pressure increases with the surface curvature according to Eq. (5):[19]

$$\ln\left(\frac{p}{p_0}\right) = \frac{V\gamma}{RT}\left(\frac{2}{r}\right) \quad (5)$$

where p is the vapour pressure over the curved surface, p_0 is the vapour pressure over a flat surface, V is the molar volume, γ is the surface tension, R is the gas constant, T is the temperature, and r is the radius.

This means that the $p\mathrm{MoO_2(OH)_2}$ is lower on the outside of the oxide, since it is in equilibrium with "large" MoO_3 particles. The $p\mathrm{MoO_2(OH)_2}$ within the oxide scale is higher because of the presence of nanometer-sized MoO_3 particles. When the vapour in the oxide with high $p\mathrm{MoO_2(OH)_2}$ reaches the oxide surface, where a lower $p\mathrm{MoO_2(OH)_2}$ prevails, some MoO_3 is re-deposited on the surface. This is illustrated schematically in Fig. 15.

3.6. Summary of results and proposal of oxidation mechanism

Our previous results showed that the oxidation rate of $MoSi_2$ increased with the partial pressure of water vapour at 450 °C in the presence of O_2.[11,12] The Mo content of the oxides decreased with increasing water vapour content in the oxidation atmosphere. It was also shown that mass loss from the MoO_3 powder started at significantly lower temperatures in oxygen that contained 10% water vapour than in dry oxygen.

Our present results show that mass gain increases in the presence of 10% water vapour at temperatures up to 470 °C and in O_2 at temperatures up to 510 °C. However, at higher temperatures, the mass gain decreased in both atmospheres. The volatilisation of Mo-containing species appears to be a key issue for the above oxidation regimes.

The interpretation of the oxidation mechanisms for the $MoSi_2$ composite in dry O_2 and $O_2 + 10\%\,H_2O$ is presented below and illustrated schematically in Fig. 16.

$MoSi_2$ oxidises to nanometer-sized crystalline MoO_3 and amorphous SiO_2, as described by reaction (1), at temperatures within the "accelerated oxidation rate region" and at higher temperatures (Fig. 16A).

$$2MoSi_2(s) + 7O_2(g) \leftrightarrow 2MoO_3(s) + 4SiO_2(s) \quad (1)$$

In dry oxygen, MoO_3 forms volatile $(MoO_3)_3$ species (6) (Fig. 16B and D). In oxygen/water vapour mixtures, the solid MoO_3 reacts with water to form the volatile $MoO_2(OH)_2$ species (4) (Fig. 16C and E). This results in the loss of Mo from the oxide scale. The vapour pressure at 500 °C of $MoO_2(OH)_2$ is 10^4-times higher than that of $(MoO_3)_3$. In other words, Mo loss from the oxide scales at this temperature is substantially greater in O_2/H_2O mixtures than in O_2.

$$MoO_3(s) + H_2O(g) \leftrightarrow MoO_2(OH)_2(g) \quad (4)$$

$$3MoO_3(s) \leftrightarrow (MoO_3)_3(g) \quad (6)$$

The higher the temperature and partial pressure of water vapour more Mo can be removed from the oxide scale. Whether or not this results in the oxide becoming more or less protective depends on the oxidation temperature.

At temperatures within the "accelerated oxidation rate region" (400–550 °C in O_2; 400–510 °C in $O_2 + 10\%\,H_2O$) the loss of Mo results in an oxide scale that has an open structure, which facilitates the penetration of oxygen through the scale (Fig. 16B and C). As a result, the oxidation rate increases. Since more Mo is lost in O_2/H_2O mixtures than in dry O_2, the oxidation rate is higher in O_2/H_2O mixtures.

At temperatures above the "accelerated oxidation rate region" (above ~550 °C in O_2; above 510 °C in $O_2 + 10\%\,H_2O$), it appears that diffusion within SiO_2 is sufficiently rapid to restructure and heal the pores that form due to Mo loss (Fig. 16F). As a result, a protective SiO_2 scale forms and the oxidation rate of $MoSi_2$ decreases (Fig. 16G). Since the vapour pressure of volatile Mo-containing species in equilibrium with MoO_3 is higher in $O_2 + 10\%\,H_2O$ than in dry O_2, enough Mo can be removed from the oxide scale at a lower temperature in O_2/H_2O mixtures than in dry O_2 for a protective SiO_2 scale to be established.

Therefore, temperatures that allow the SiO_2 scale to heal the pores that result from the removal of Mo from the oxide are beneficial, whereas temperatures at which the SiO_2 scale cannot heal these pores speed up oxidation.

4. Conclusions

The oxidation behaviour of a clay-bonded $MoSi_2$-based composite was examined. The peak oxidation rates of the $MoSi_2$ composite in dry O_2 and $O_2 + 10\%\,H_2O$ occurred at temperatures of about 510 and 470 °C, respectively. At higher temperatures, the oxidation rate decreased in both atmospheres. The decrease was steeper and occurred at a lower temperature in $O_2 + 10\%\,H_2O$ than in O_2.

We have shown that the depletion of Mo from oxide scales during oxidation is more pronounced with increasing temperature and water vapour content. The evaporation of a Mo-containing species is evidenced by the formation of MoO_3 deposits in the cooler parts of the exposure tube. Mo transport probably takes place via the formation of volatile $MoO_2(OH)_2$ in the presence of water vapour. It appears that the key process is Mo loss, which influences the protective properties of the oxide layer that is formed on $MoSi_2$.

The following mechanism is proposed to explain the different oxidation rates in O_2 and $O_2 + 10\%\,H_2O$: $MoSi_2$ oxidises to MoO_3 and SiO_2; in O_2/H_2O mixtures, the solid MoO_3 reacts with water to form volatile $MoO_2(OH)_2$ species, whereas in dry O_2, MoO_3 tends to form the volatile $(MoO_3)_3$ species; this results in the loss of Mo from the oxide. Since the vapour pressure within the investigated temperature range of $MoO_2(OH)_2$ is at least 10^3-fold higher

than that of $(MoO_3)_3$, substantially higher Mo loss occurs in O_2/H_2O mixtures than in O_2.

At temperatures within the "accelerated oxidation rate region", the loss of Mo leaves the oxide with an open structure, which facilitates the diffusion of oxygen through the oxide scale, thereby increasing the rate of oxidation. Since more Mo is lost in O_2/H_2O mixtures, the oxidation rate is higher in O_2/H_2O than in dry O_2.

At temperatures above the "accelerated oxidation rate region", it appears that diffusion within SiO_2 is rapid enough to restructure and heal the pores that are formed due to Mo loss. As a result, a protective SiO_2 scale forms and the oxidation rate of $MoSi_2$ decreases. The protective SiO_2 scale can form at a lower temperature in O_2/H_2O mixtures than in dry O_2, since more Mo is lost in the presence of water vapour. This results in decreased oxidation rates at lower temperatures in O_2/H_2O mixtures than in dry O_2.

Acknowledgements

This work was carried out within the High-Temperature Corrosion Center (HTC) at Chalmers, Sweden.

References

1. Meschter, P. J., Low-temperature oxidation of molybdenum disilicide. *Metallurg. Trans. A* 1992, **23A**, 1763–1772.
2. Schlichting, J., Molybdändisilizid als Komponente morderner Hochtemperatur-verbundwerkstoffe. *High Temp. High Pressures* 1978, **10**, 241–269.
3. Bertiss, D. A., Cerchiara, R. R., Gulbransen, E. A., Pettit, F. S. and Meier, G. H., Oxidation of $MoSi_2$ and comparison with other silicide materials. *Mater. Sci. Eng.* 1992, **A155**, 165–181.
4. Fitzer, V. E., Molybdändisilizid als hochtemperaturwerkstoff. In *Proceedings of 2nd Plansee Seminar*, ed. F. Benesovsky. Springer, Pergamon Press, Berlin, 1965, 1955, pp. 56–79.
5. Chou, T. C. and Nieh, T. G., Pesting of the high-temperature intermetallic $MoSi_2$. *JOM* 1993, **45**, 15–21.
6. Wirkus, C. D. and Wilder, D. R., High-temperature oxidation of molybdenum disilicide. *J. Am. Ceram. Soc*. 1966, **49**, 173–177.
7. Berkowitz-Mattuck, J. B., Blackburn, P. E. and Felten, E. J., The intermediate-temperature oxidation behaviour of molybdenum disilicide. *Trans. Metallurg. Soc. Aime* 1965, **233**, 1093–1099.
8. Chou, T. C. and Nieh, T. G., New observations of $MoSi_2$ pest at 500 °C. *Script. Metallurg. Mater.* 1992, **26**, 1637–1642.
9. Kurakowa, K., Houzumi, H., Saeki, I. and Takahashi, H., Low temperature oxidation of fully dense and porous $MoSi_2$. *Mater. Sci. Eng.* 1999, **A261**, 292–299.
10. Millner, T. and Neugebauer, J., Volatility of the oxides of tungsten and molybdenum in the presence of water vapour. *Nature* 1949, **163**, 601–602.
11. Hansson, K., Svensson, J.-E., Halvarsson, M., Tang, J. E., Sundberg, M. and Pompe, R., The influence of water vapour on the oxidation of $MoSi_2$ at 450° C. *Mater. Sci. Forum* 2001, **369–372**, 419–426.
12. Hansson, K., Halvarsson, M., Tang, J. E., Svensson, J.-E., Sundberg, M. and Pompe, R., On the mechanism of $MoSi_2$ pesting in the temperature range 400–500 °C. In *Ceramic Engineering and Science Proceeding (CESP), Vol 21* (*Issue 4*), eds. T. Jessen and E. Ustundag, 2000, pp. 469–476.
13. Tang, J. E., Halvarsson, M., Hansson, K., Svensson, J.-E. and Sundberg, M., An investigation of the microstructure in the pest oxide of a $MoSi_2$-based composite. In *Ceramic Engineering and Science Proceeding (CESP), Vol 21* (*Issue 4*), eds. T. Jessen and E. Ustundag, 2000, pp. 477–484.
14. Berkowitz, J. and Inghram, M. G., Polymeric gaseous species in the sublimation of molybdenum trioxide. *J. Chem. Phys.* 1957, **26**, 842–846.
15. Glemser, V. O. and Haeseler, R. V., *Uber Gasförmige Hydroxide des Molybdäns und Wolframs. Zeitschrift fur Anorganische und Allgemeine Chemie, Band 316*, 1962.
16. Barin, I., *Thermochemical Data of Pure Substances*, VCH Verlagsgesellschaft mbh, 1995.
17. *NIST-JANAF Thermochemical Tables* (*4th ed.*), J. Phys. Chem. Ref. Data, Monograph 9, 1998.
18. Johnson, J.R.T. and Panas, I., Hydrolysis on transition metal oxide clusters and the stabilities of M–O–M Bridges. *Inorg. Chem.* 2000, **39**, 3192–3204.
19. Kingery, W.D., *Introduction to Ceramics*, John Wiley & Sons, Inc., 1960.